Solution NMR Studies and Crystal Structure of the Water-Soluble Iron(III) Porphyrin Iron 5,10,15,20-Tetrakis(2,3,5,6-tetrafluoro-4-*N*,*N*,*N*-trimethylaniliniumyl)porphyrin ([FeTF$_4$TMAP]$^{5+}$)

Timothy La,[1a] Gordon M. Miskelly,*[,1b] and Robert Bau[1a]

Departments of Chemistry, University of Southern California, Los Angeles, California 90089, and University of Auckland, Private Bag 92019, Auckland, New Zealand

Received December 13, 1996[⊗]

The crystal structure of [Fe^{III}(TF$_4$TMAP)(H$_2$O)$_2$](CF$_3$SO$_3$)$_5$·2CH$_3$CN·2H$_2$O (a = 13.065(2) Å, b = 13.375(2) Å, c = 13.839(2) Å, α = 110.97°, β = 104.97°, γ = 94.22°, V = 2144.2(6) Å^3, Z = 1) shows that the Fe(III) has two axial coordinated waters. This is in accord with solution NMR results which show that small concentrations of water (>5%) in an acetonitrile solution displace the $CF_3SO_3^-$ ligand from the iron(III) porphyrin. The ^{19}F NMR spectra of an acetonitrile solution of the hydroxo form of this Fe(III) porphyrin show changes as the water content increases above 70% which are interpreted as indicating a change from five-coordinate [Fe^{III}(TF$_4$TMAP)-OH]$^{4+}$ to six-coordinate [Fe^{III}(TF$_4$TMAP)(H$_2$O)OH]$^{4+}$. Variable-temperature ^{19}F NMR has been used to analyze the slow interconversion of [Fe^{III}(TF$_4$TMAP)(H$_2$O)$_2$]$^{5+}$ and [Fe^{III}(TF$_4$TMAP)OH]$^{4+}$. The kinetic results suggest that interconversion occurs mainly via bimolecular reaction between the aqua and hydroxo forms with $k = 1.6 \times 10^6$ M^{-1} s^{-1} (298 K) and $E_a = 6.7 \pm 0.4$ kcal mol^{-1}. This rate constant is significantly smaller than the reported interconversion rate constants for other aqua/hydroxo complexes.

Introduction

In a previous paper we reported that the interconversion of [Fe^{III}(TF$_4$TMAP)(H$_2$O)$_2$]$^{5+}$ and [Fe^{III}(TF$_4$TMAP)OH]$^{4+}$, Figure 1,[2] is slow on the NMR time scale at room temperature in mixed acetonitrile−water solutions.[3] Previous studies have indicated that interconversion of aqua- and hydroxoiron(III) porphyrins in buffered aqueous solution is usually fast on the NMR,[4] cyclic voltammetric (<1 V s^{-1}),[5−8] and stopped-flow[9−11] time scales. Given the recent reports of slow protonation of μ-oxo porphyrin dimers,[12,13] it was decided that a more detailed study of the [Fe^{III}(TF$_4$TMAP)]$^{n+}$ system was desirable.

Proton transfer in aqueous solution can be explained in terms of reactions 1−3 where reaction 3 may involve solvent

$$HA^{n+} + H_2O \underset{k_{-1}}{\overset{k_1}{\rightleftharpoons}} A^{(n-1)+} + H_3O^+ \quad (1)$$

$$HA^{n+} + OH^- \underset{k_{-2}}{\overset{k_2}{\rightleftharpoons}} A^{(n-1)+} + H_2O \quad (2)$$

$$HA^{n+} + A^{(n-1)+} \underset{k_{-3}}{\overset{k_3}{\rightleftharpoons}} A^{(n-1)+} + HA^{n+} \quad (3)$$

participation.[14] Reactions 1 and 2 usually occur at a diffusion-controlled rate in the favorable direction if the site of protonation

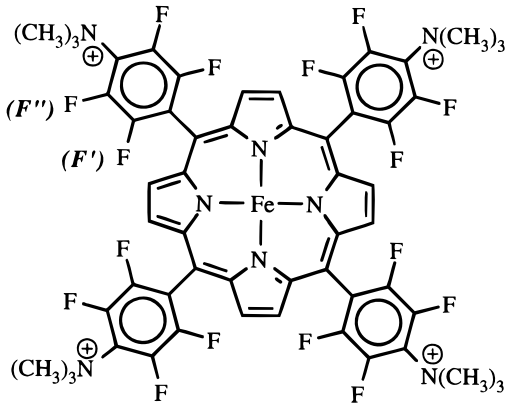

Figure 1. Diagram of [Fe^{III}(TF$_4$TMAP)]$^{5+}$ (axial ligands not shown).

is at oxygen or nitrogen (assuming pK_a(H$_3$O$^+$) ≪ pK_a(HA^{n+}) ≪ pK_a(H$_2$O)), with the reverse rate being controlled by the requirement that $k_1/k_{-1} = K_a$ and $k_2/k_{-2} = K_a/K_w$, where K_a is the acid dissociation constant for HA^{n+} and K_w is the water autoionization constant.[14] The assumption that pK_a(H$_3$O$^+$) ≪ pK_a(HA^{n+}) ≪ pK_a(H$_2$O) means that at equilibrium reaction 1 lies far to the left with a diffusion-controlled rate in the reverse direction of k_{-1}[A$^{(n-1)+}$][H$_3$O$^+$] while reaction 2 lies to the right with a diffusion-controlled forward rate of k_2[HA^{n+}][OH$^-$]. In solutions containing significant concentrations of HA^{n+} and A$^{(n-1)+}$ reaction 3 can represent a major mechanism for proton transfer,[14] especially when 9 > pK_a(HA^{n+}) > 5. This is because

⊗ Abstract published in *Advance ACS Abstracts,* October 1, 1997.

(1) (a) University of Southern California. (b) University of Auckland.

(2) Abbreviations used for coordinated porphyrins: TF$_4$TMAP, 5,10,15,20-tetrakis(2,3,5,6-tetrafluoro-4-*N*,*N*,*N*-trimethylaniliniumyl)porphyrinato; TPP, 5,10,15,20-tetraphenylporphyrinato; T(4-NMePyP), 5,10,15,20-tetrakis(4-*N*-methylpyridiniumyl)porphyrinato. ^{1}H and ^{2}H are used to specify the isotopes of hydrogen. H is used when either ^{1}H or ^{2}H could be present.

(3) La, T.; Miskelly, G. M. *J. Am. Chem. Soc.* **1995**, *117*, 3613−3614.
(4) Ivanca, M. A.; Lappin, A. G.; Scheidt, W. R. *Inorg. Chem.* **1991**, *30*, 711−718.
(5) Kurihara, H.; Arifuku, F.; Ando, I.; Saita, M.; Nishino, R.; Ujimoto, K. *Bull. Chem. Soc. Jpn.* **1982**, *55*, 3515−3519.
(6) Webley, W. S. Ph.D. Thesis, University of Otago, Dunedin, 1984.
(7) Miskelly, G. M. Ph.D. Thesis, University of Otago, Dunedin, 1986.
(8) Cheng, S.-M.; Sun, P.-J.; Su, Y. O. *J. Electroanal. Chem.* **1990**, *294*, 151−164.
(9) El Awady, A. A.; Wilkins, P. C.; Wilkins, R. G. *Inorg. Chem.* **1985**, *24*, 2053−2057.
(10) Tondreau, G. A.; Wilkins, R. G. *Inorg. Chem.* **1986**, *25*, 2745−2750.
(11) Miskelly, G. M.; Webley, W. S.; Clark, C. R.; Buckingham, D. A. *Inorg. Chem.* **1988**, *27*, 3773−3781.
(12) Carroll, J. M.; Norton, J. R. *J. Am. Chem. Soc.* **1992**, *114*, 8744−8745.
(13) Kramarz, K. W.; Norton, J. R. *Prog. Inorg. Chem.* **1994**, *42*, 1−65.
(14) Bell, R. P. *The Proton in Chemistry*; Cornell University Press: Ithaca, NY, 1973.

S0020-1669(96)01486-3 CCC: $14.00

even though the reverse of reaction 1 is diffusion controlled the rate is dependent on $[H_3O^+]$ so that if $[H_3O^+] < 10^{-5}$ mol L^{-1} the pseudo-first-order rate constant for protonation of $A^{(n-1)+}$ will be $<10^{-5}$ s^{-1} (assuming a diffusion-controlled bimolecular rate constant of ca. 10^{10} mol^{-1} L s^{-1}). A similar argument holds for the forward direction of reaction 2.

Early studies of aquated metal complexes suggested that protonation and deprotonation of coordinated hydroxide and water respectively occur in accord with the above "normal" expectations, with the thermodynamically-favored reaction (usually corresponding to the reverse of reaction 1) occurring at close to a diffusion-controlled rate.[15−18] Few studies have included conditions where both the aqua and hydroxo forms of a given complex coexist in significant concentrations in solution.[19,20] However, other studies have shown an increase in the rate of proton exchange between coordinated and bulk water as the pH increases, suggesting that reaction 3 is a rapid process.[21−23] Thus, Fong and Grunwald estimated that k_3 for the aquated Al^{3+} system was 9×10^8 M^{-1} s^{-1} at 29.9 °C.[22] It is not possible to confirm the presence of pathway 3 from results reported in the other cited papers because experiments were usually performed at only one concentration of complex and therefore cannot distinguish between paths 2 and 3 (or, indeed, further deprotonations) as the cause of the increased exchange rate at higher pH.[23,24] The only direct measurement of the rate of reaction 3 in a solution containing large amounts of both aqua and hydroxo species is a study of $[M(O)(H_2O)(CN)_4]^{3-}$ and $[M(O)(OH)(CN)_4]^{4-}$ (M = Mo(IV) or W(IV)) which obtained values for k_3 of $>1 \times 10^7$ M^{-1} s^{-1}.[19] In apparent contrast to this result a recent study reports that protons in the first coordination sphere of $[Rh(H_2O)_6]^{3+}$ are in slow exchange with bulk water even in solutions containing equal concentrations of $[Rh(H_2O)_6]^{3+}$ and $[Rh(H_2O)_5(OH)]^{2+}$, which would suggest a slow interconversion between aqua and hydroxo complexes.[20] However, this study notes that these complexes have a highly ordered second coordination sphere[25,26] and proposes that protonation of a ligand in the first coordination sphere could occur without direct incorporation of a proton from the bulk solvent.[20,22]

The complexes mentioned in the previous paragraph are unlikely to change their coordination geometries dramatically during proton transfer so that it is not surprising that these complexes tend to behave like "typical" oxygen acids and bases. However, the coordination geometries of the "aqua" and "hydroxo" forms of an iron(III) porphyrin are not necessarily similar. There is little doubt that in most aqueous systems the aquairon porphyrin is the six-coordinate diaqua species, as indicated by crystal structures,[27−30] Raman studies,[31−33] and NMR studies.[4,33,34] However, the identity of the hydroxo form is much less certain. In poorly-coordinating organic solvents the hydroxoiron(III) porphyrin is best described as five-coordinate, with a structure and properties similar to those of species such as the chloroiron(III) porphyrins.[3,35−37] However, there is some uncertainty whether this is still the case in aqueous solutions or whether water coordinates significantly to the other side of the iron(III) center and, if it is coordinated, how strong the interaction is and whether it affects the geometry about the iron.[11] Related to this coordination ambiguity is the identification of the observed second acid dissociation constant, K_{a2}, of an iron(III) porphyrin as corresponding to deprotonation of a coordinated water, eq 4, or binding of a hydroxide, eq 4a. The latter equation has precedent in the "acid dissociation" of species such as $B(OH)_3$.

$$[Fe(TF_4TMAP)(H_2O)(OH)]^{4+} = [Fe(TF_4TMAP)(OH)_2]^{3+} + H^+ \quad (4)$$

$$[Fe(TF_4TMAP)OH]^{4+} + OH^- = [Fe(TF_4TMAP)(OH)_2]^{3+} \quad (4a)$$

The current paper uses information gleaned from variable-temperature NMR and experiments in solutions of differing water content to suggest an explanation for the slowness of the interconversion of $[Fe^{III}(TF_4TMAP)(H_2O)_2]^{5+}$ and $[Fe^{III}(TF_4TMAP)OH]^{4+}$. As mentioned briefly previously,[3] the interconversion rate is probably limited by molecular rearrangement in the iron(III) porphyrin.

Experimental Section

Materials. All organic solvents were of AR grade and were used as supplied. $LiCF_3SO_3$ (Aldrich), $^2H_3$-acetonitrile (Aldrich), and ^2H_2O (Aldrich) were used as supplied. Water was deionized (18 MΩ) with a Barnstead Nanopure system.

Synthesis. $[Fe^{III}(TF_4TMAP)](CF_3SO_3)_5$ was prepared as described previously.[38] It was recrystallized by diffusing ether into a solution of iron porphyrin in CH_3CN. This material could be dried at room temperature under vacuum to give a material which low-temperature NMR showed contained coordinated $CF_3SO_3^-$.[3,38] Anal. Calcd for

(15) Hemmes, P.; Rich, L. D.; Cole, D. L.; Eyring, E. M. *J. Phys. Chem.* **1970**, *74*, 2859−2862.
(16) Hemmes, P.; Rich, L. D.; Cole, D. L.; Eyring, E. M. *J. Phys. Chem.* **1971**, *75*, 929−932.
(17) Holmes, L. P.; Cole, D. L.; Eyring, E. M. *J. Phys. Chem.* **1968**, *72*, 301−304.
(18) Rich, L. D.; Cole, D. L.; Eyring, E. M. *J. Phys. Chem.* **1969**, *73*, 713−716.
(19) Roodt, A.; Leipoldt, J. G.; Helm, L.; Merbach, A. E. *Inorg. Chem.* **1994**, *33*, 140−147.
(20) Banyai, I.; Glaser, J.; Read, M. C.; Sandstrom, M. *Inorg. Chem.* **1995**, *34*, 2423−2429.
(21) Takahashi, A. *J. Phys. Soc. Jpn.* **1970**, *28*, 207−214.
(22) Fong, D.-W.; Grunwald, E. *J. Am. Chem. Chem. Soc.* **1969**, *91*, 2413−2422.
(23) Wang, K.; Jordan, R. B. *Inorg. Chem.* **1993**, *32*, 895−897.
(24) Swift, T. J.; Stephenson, T. A. *Inorg. Chem.* **1966**, *5*, 1100−1104.
(25) Easteal, A. J.; Mills, R.; Woolf, L. A. *J. Phys. Chem.* **1989**, *93*, 4968−4972.
(26) Read, M. C.; Sandstrom, M. *Acta Chem. Scand.* **1992**, *46*, 1177−1182.
(27) Korber, F. C. F.; Lindsay Smith, J. R.; Prince, S.; Rizkallah, P.; Reynolds, C. D.; Shawcross, D. R. *J. Chem. Soc., Dalton Trans.* **1991**, 3291−3294. The authors noted that all attempts to collect data on their crystal (V = ca. 10^{-4} mm^3) by conventional means were unsuccessful. Data were collected using a synchotron X-ray source instead.
(28) (a) Kastner, M. E.; Scheidt, W. R.; Mashiko, T.; Reed, C. A. *J. Am. Chem. Soc.* **1978**, *100*, 666−667. (b) Scheidt, W. R.; Cohen, I. A.; Kastner, M. E. *Biochemistry* **1979**, *18*, 3546−3552.
(29) Ceccio, S. M. M.Sc. Thesis, Univ. of California at Los Angeles, Los Angeles, 1988.
(30) Cheng, B.; Scheidt, W. R. *Acta Crystallogr.* **1995**, *C51*, 1271−1275.
(31) Bell, S. E. J.; Hester, R. E.; Hill, J. N.; Shawcross, D. R.; Lindsay Smith, J. R. *J. Chem. Soc., Faraday Trans.* **1990**, *86*, 4017−4023.
(32) Reed, R. A.; Rodgers, K. R.; Kushmeider, K.; Spiro, T. G.; Su, Y. O. *Inorg. Chem.* **1990**, *29*, 2881−2883.
(33) Rodgers, K. R.; Reed, R. A.; Su, Y. O.; Spiro, T. G. *Inorg. Chem.* **1992**, *31*, 2688−2700.
(34) Zobrist, M.; La Mar, G. N. *J. Am. Chem. Soc.* **1978**, *100*, 1944−1946.
(35) Cheng, R.-J.; Latos-Grazynski, L.; Balch, A. L. *Inorg. Chem.* **1982**, *21*, 2412−2418.
(36) Gunter, M. J.; McLaughlin, G. M.; Berry, K. J.; Murray, K. S.; Irving, M.; Clark, P. E. *Inorg. Chem.* **1984**, *23*, 283−300.
(37) Woon, T. C.; Shirazi, A.; Bruice, T. C. *Inorg. Chem.* **1986**, *25*, 3845−3846.
(38) (a) La, T.; Richards, R.; Miskelly, G. M. *Inorg. Chem.* **1994**, *33*, 3159−3163. (b) La, T.; Richards, R. A.; Lu, R. S.; Bau, R.; Miskelly, G. M. *Inorg. Chem.* **1995**, *34*, 5632−5640.

Table 1. Crystal and Data Collection Parameters for $[Fe^{III}(TF_4TMAP)(H_2O)_2](CF_3SO_3)_5\cdot 2CH_3CN\cdot 2H_2O$

formula	$C_{65}H_8F_{31}N_{10}O_{20}S_5$
cryst size (mm)	0.3 × 0.3 × 0.4
MW	2054.0
space group	*P*1
a (Å)	13.065(2)
b (Å)	13.375(2)
c (Å)	13.839(2)
α (deg)	110.97(2)
β (deg)	104.97(2)
γ (deg)	94.22(2)
V (Å^3)	2144.2(6)
Z	1
T (K)	173
radiation	Cu Kα (graphite monochromator)
2*θ* range (deg)	2.0−102.5
scan type	*ω*
scan speed	variable; 8.00−60.00°/min in *ω*
no. of reflcns collcd	5043
no. of indepndt reflcns	4296
unique reflcns used in least-squares fit	3178 ($F > 5.0\sigma(F)$)
R on F_o for data with $F_o > 5\sigma(F_o)$	14.72%
R_w on F_o for data with $F_o > 5\sigma(F_o)$	15.60%

$[Fe(TF_4TMAP)](CF_3SO_3)_5(H_2O)_4$: C, 36.52; H, 2.61; N, 5.58. Found: C, 36.49; H, 2.52; N, 5.59.

$[Fe^{III}(TF_4TMAP)OH](CF_3SO_3)_4$. $[Fe^{III}(TF_4TMAP)](CF_3SO_3)_5$ (30 mg; 0.015 mmol) was dissolved in 160 mL of 1:1 CH_3CN-H_2O. The pH of the solution was adjusted to >9 resulting in a color change from dark green to dark red. $LiCF_3SO_3$ (ca. 0.3 g) was added, the solution was filtered, and the volume was reduced by slow evaporation (Rotavapor) to give a dark red precipitate. This material was filtered and washed with water and then air dried. The dark red solid was dissolved in 1:1 CH_3CN-H_2O (160 mL), $LiCF_3SO_3$ (ca. 0.3 g) was added, the solution was filtered, and the volume was again reduced until the microcrystalline solid formed. UV−vis (CH_3CN): 335, 420, and 560 nm. ^{1}H NMR (C^2H_3CN): 82.7 (br, s, 8H, *β*-pyrrole H) and 4.53 (s, 36H, $N^+(CH_3)_3$) ^{19}F{^{1}H} NMR (C^2H_3CN): −78.0 (s, 12F, $CF_3SO_3^-$), −112.9 (br, s, 8F, F′), −130.7 (br, s, 4F, F″), −132.0 (br, s, 4F, F″).

{$[Fe^{III}(TF_4TMAP)]_2O(CF_3SO_3)_8$}. $[Fe^{III}(TF_4TMAP)](CF_3SO_3)_5$ (ca. 40 mg) was dissolved in 1:1 CH_3CN-H_2O (40 mL), $LiCF_3SO_3$ (ca. 60 mg) was added, the solution was filtered, and the volume was slowly reduced to yield a dark brown precipitate. The precipitate was redissolved by adding CH_3CN (20 mL), and the volume was again reduced to give a dark brown solid which turned brick red upon removal of the solvent. The solid was washed with H_2O, 2-propanol/diethyl ether, and diethyl ether and was then air dried. Yield: 85%. UV−vis (CH_3CN): 322, 395, 440 (sh), and 557 nm. ^{1}H NMR (C^2H_3CN): 14.3 (br, s, 16H, *β*-pyrrole H) and 4.13 (s, 72 H, $N^+(CH_3)_3$). ^{19}F{^{1}H} NMR (C^2H_3CN): −78.0 (s, 24F, $CF_3SO_3^-$), −131.1 (br, s, 8F, F'), −134.0 (br, s, 8F, F′), −137.4 (s, 8F, F″), −138.9 (s, 8F, F″).

The Cl^- salt of $[Fe^{III}(TF_4TMAP)]^{5+}$ could be prepared by dissolution of $[Fe^{III}(TF_4TMAP)](CF_3SO_3)_5$ in acetone and addition of Bu_4NCl. This material could not be dried completely because this led to demethylation of the quaternary trimethylanilinium group.

Crystal Structure of $[Fe^{III}(TF_4TMAP)(H_2O)_2](CF_3SO_3)_5\cdot 2CH_3CN\cdot 2H_2O$. Single crystals of $[Fe^{III}(TF_4TMAP)(H_2O)_2](CF_3SO_3)_5\cdot 2CH_3CN\cdot 2H_2O$ were grown by slow diffusion of toluene into a saturated solution of the iron porphyrin in wet 1:1 CH_3CN−acetone in a 5 mm o.d. glass NMR tube. A dark purple-red crystal was mounted on a Siemens P4/RA automatic diffractometer. Data were collected at low temperature (−100 °C) to avoid solvent loss. Three standard reflections were measured after every 100 data points collected and did not show any significant deviation. A total of 3178 reflections had $F_o > 5\sigma(F_o)$ and were used in all subsequent calculations. Final cell constants as well as other information related to data collection and refinement are listed in Table 1. All calculations were made using the Siemens SHELXTL program.[39] The structure of $[Fe^{III}(TF_4TMAP)(H_2O)_2](CF_3SO_3)_5\cdot 2CH_3CN\cdot 2H_2O$ was solved by direct methods,[40] which revealed the atomic coordinates of one porphyrin molecule in the unit cell. Calculated hydrogen atoms were entered and constrained to riding motions with fixed isotropic displacement coefficients (*U*).

Attempts to grow X-ray-quality crystals of the other iron porphyrin derivatives were not successful.

Solution Studies. The ^{1}H and ^{19}F NMR spectra were measured in 5 mm tubes on Bruker AC-F250 and AM-360 spectrometers. ^{1}H spectra are referenced to TMS, and ^{19}F spectra are referenced to $CFCl_3$. Variable-temperature NMR (VT-NMR) temperatures were calculated using 4% CH_3OH in $C^2H_3O^2H$ and 80% glycol in dimethyl-d_6 sulfoxide mixtures as external standards. Where necessary NaO^2H solutions were prepared by dissolving the required amount of solid NaOH in ^2H_2O. All mixed solvent compositions are given as volume:volume ratios prior to mixing. Where water concentrations are given in molarities, these are approximate and have been calculated ignoring excess volumes of mixing or density changes with temperature.

The chemical shift and full width at half-maximum (fwhm) values for most ^{19}F NMR peaks were obtained by the program NUTS (Acorn), but the values for the ortho fluorines of $[Fe(TF_4TMAP)OH]^{4+}$ were obtained by fitting the observed spectra to two lorentzians of equal area but different positions and line widths, using the program Kaleidagraph 3.0 (Synergy). These fits gave reasonable results for most NMR spectra except for the low-temperature (<260 K) spectra for $[Fe(TF_4TMAP)(O^2H)]^{4+}$, where the ortho fluorines were insufficiently separated for unambiguous resolution.

Simulations. Simulations of the variable-temperature (VT) ^{19}F NMR experiments were performed using the matrix technique suggested by Sack[41] as reported by Binsch.[42] This method is designed to work for simple noncoupled nonsaturated nuclei undergoing chemical exchange. The kinetic broadening of the resonances due to the ortho (F′) and meta (F″) fluorines were calculated separately, and the calculated spectra were obtained by adding the spectral contributions from the separate calculations in the region −125 to −135 ppm. This region includes the ^{19}F NMR signals for the ortho and meta fluorines of $[Fe^{III}(TF_4TMAP)(H_2O)_2]^{5+}$ and the meta fluorines of $[Fe^{III}(TF_4TMAP)OH]^{4+}$. The ^{19}F NMR signals for the ortho fluorines of $[Fe^{III}(TF_4TMAP)OH]^{4+}$ are not plotted in this paper because they are sufficiently broad that the kinetics do not alter their shape much, and they are sufficiently far away that their inclusion in the spectra would decrease the resolution of the more informative region near −130 ppm. The effect of the ortho fluorines of $[Fe^{III}(TF_4TMAP)OH]^{4+}$ was, however, included in the calculation of the shape of the resonance corresponding to the ortho fluorines of $[Fe^{III}(TF_4TMAP)(H_2O)_2]^{5+}$. The treatment of the ortho and meta fluorines was identical; that for the meta fluorines was as follows:

The problem to be modeled can be represented as

$$A \underset{k_{BA}}{\overset{k_{AB}}{\rightleftharpoons}} B \underset{k_{A'B}}{\overset{k_{BA'}}{\rightleftharpoons}} A'$$

where A and A′ are the two meta ^{19}F environments in the hydroxo porphyrin, B is the meta environment in the diaqua form, and k_{AB} is the first-order rate constant for transformation of ^{19}F from site A to site B. As defined, k_{AB} will also be equal to the pseudo-first-order rate constant (k') for conversion of the hydroxo form of the iron(III) porphyrin into the diaqua form during the process

$$[Fe(TF_4TMAP)(H_2O)_2]^{5+} + [Fe(TF_4TMAP)OH]^{4+} \rightleftarrows [Fe(TF_4TMAP)OH]^{4+} + [Fe(TF_4TMAP)(H_2O)_2]^{5+} \quad (5)$$

Therefore, $f_B = f_{H_2O}$, $f_A = f_{A'} = f_{OH}/2$, and $k' = k_{AB} = k_{A'B} = k_{BA}(2f_{H_2O}/f_{OH}) = k_{BA'}(2f_{H_2O}/f_{OH})$, where f_A, $f_{A'}$, and f_B are the fractions of relevant ^{19}F nuclei in sites A, A′, and B, respectively, f_{OH} is the

(39) Sheldrick, G. M. *SHELX-76*; University of Cambridge: Cambridge, U.K., 1976.
(40) Sheldrick, G. M. *SHELX-86*; University of Gottingen: Gottingen, Germany, 1986.
(41) Sack, R. A. *Mol. Phys.* **1958**, *1*, 163.
(42) Binsch, G. In *Dynamic Nuclear Magnetic Resonance Spectroscopy*; Jackman, L. M., Cotton, F. A., Eds.; Academic Press: New York, 1975; pp 45−81.

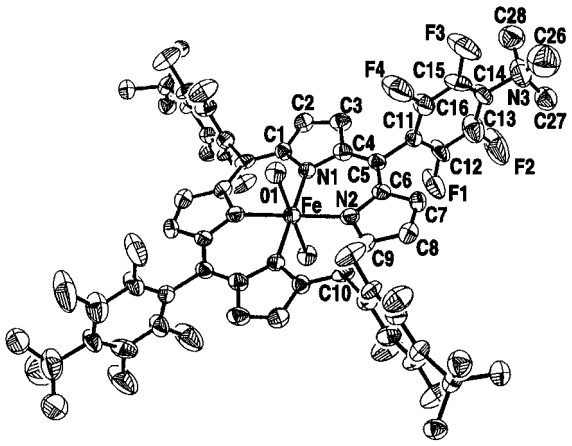

Figure 2. ORTEP drawing of the porphyrin cation in $[Fe^{III}(TF_4TMAP)(H_2O)_2](CF_3SO_3)_5 \cdot 2H_2O \cdot 2CH_3CN$ showing positions of the aromatic substituents and partial numbering of the atoms. The iron atom is situated on a crystallographic center of symmetry.

fraction of porphyrin in the hydroxo form, and f_{H_2O} is the fraction of porphyrin in the aqua form ($f_{OH} + f_{H_2O} = 1$). It must be stressed that eq 5 does not imply a rate law or mechanism but rather shows the overall reaction for interconversion of the aqua and hydroxo iron porphyrins and thereby interconversion of the fluorine sites. This reaction may have a rate unimolecular in iron(III) porphyrin (cf. eqs 1 and 2) or bimolecular in iron(III) porphyrin (cf. eq 3). The order of the reaction with respect to porphyrin is irrelevant for the initial analysis because all concentrations are constant during the NMR studies (the system is at equilibrium) so that the observed rate of interconversion is pseudo-first-order.

The parameters varied in the fit were an arbitrary intensity multiplier, the fraction of porphyrin present as the hydroxo species (f_{OH}), and the pseudo-first-order rate constant for conversion of the hydroxo form into the aqua form ($k' = k_{AB}$). The reverse rate constant and fractions of ^{19}F in each site were calculated from these latter two parameters using the above equations. Peak positions and peak widths for the species in the absence of chemical reaction were obtained from VT NMR studies of the isolated $[Fe^{III}(TF_4TMAP)(H_2O)_2]^{5+}$ and $[Fe^{III}(TF_4TMAP)OH]^{4+}$ systems.

Since the system is comparatively simple (two sets of 3 types of nuclei), no effort was made to optimize the computation. The matrix manipulations were performed using MathCad 3 (Mathsoft), and the parameters f_{OH} and k_{AB} were varied until a satisfactory fit was obtained as evaluated by visual comparison of the observed and simulated data. All calculations were performed on a Macintosh Powerbook 160 with Digital Eclipse daughterboard (33 MHz 68030 with 68882 FPU). Experimental ^{19}F NMR spectra in the region -125 to -135 ppm were digitized and baseline-corrected before comparison with the simulated data.

Results

X-ray Crystal Structure. The crystal structure of the porphyrin component of $[Fe^{III}(TF_4TMAP)(H_2O)_2](CF_3SO_3)_5(CH_3CN)_2(H_2O)_2$ is illustrated in Figure 2. The crystal has a one molecule in a triclinic unit cell. Final cell constants as well as other information related to data collection and refinement are reported in Table 1. As is common with many water-soluble porphyrin structures,[4] the structure is of poor quality due to disorder of the solvent and counterions. Nevertheless, the structure of the porphyrin cation is still well-defined and confirms our assignment of this species as a six-coordinate diaquairon porphyrin. The iron atom is positioned precisely in the plane of the porphyrinato ligand (at the crystallographic center of inversion) with the porphyrin having a slight distortion into local C_{2v} symmetry. A figure showing the relative positions of the atoms in the porphyrin skeleton and their displacement from the rms plane of the porphyrin ring N atoms is included in the Supporting Information. Table 2 displays selected bond distances and angles in the porphyrin cation.

Table 2. Selected Bond Lengths (Å) and Angles (deg) in the $[Fe^{III}(TF_4TMAP)(H_2O)_2]^{5+}$ Cation

Bond Lengths[a]			
Fe−N(1)	2.046(14)	Fe−N(2)	2.037(15)
Fe−O(1)	2.090(8)	N(1)−C(1)	1.355(25)
N(1)−C(4)	1.375(22)	N(2)−C(6)	1.378(21)
N(2)−C(9)	1.404(25)	C(1)−C(2)	1.412(25)
C(2)−C(3)	1.357(28)	C(3)−C(4)	1.441(27)
C(4)−C(5)	1.382(27)	C(5)−C(6)	1.412(26)
C(6)−C(7)	1.417(27)	C(7)−C(8)	1.364(26)
C(8)−C(9)	1.429(25)	C(9)−C(10)	1.382(24)
C(5)−C(11)	1.495(23)	C(11)−C(12)	1.362(20)
C(12)−C(13)	1.398(27)	C(13)−C(14)	1.362(18)
C(14)−C(15)	1.346(18)	C(15)−C(16)	1.381(26)
C(16)−C(11)	1.318(20)	C(10)−C(17)	1.486(27)
C(17)−C(18)	1.347(20)	C(18)−C(22)	1.381(29)
C(22)−C(19)	1.421(18)	C(19)−C(20)	1.334(16)
C(20)−C(21)	1.377(28)	C(21)−C(17)	1.402(22)
C(14)−N(3)	1.510(14)	N(3)−C(23)	1.470(17)
N(3)−C(25)	1.483(22)	N(3)−C(27)	1.480(15)
C(19)−N(4)	1.506(15)	N(4)−C(29)	1.481(17)
N(4)−C(31)	1.482(18)	N(4)−C(33)	1.472(16)
C(14)−N(3)	1.510(14)	N(3)−C(23)	1.470(17)

Bond Angles[a]			
O(1)−Fe−N(1)	89.8(4)	O(1)−Fe−N(2)	89.6(5)
N(1)−Fe−N(2)	89.8(6)	Fe−N(1)−C(1)	127.5(11)
Fe−N(1)−C(4)	125.9(13)	Fe−N(2)−C(6)	127.9(13)
Fe−N(2)−C(9)	125.2(11)	C(1)−N(1)−C(4)	106.4(14)
C(6)−N(2)−C(9)	106.9(14)	C(4)−C(5)−C(6)	126.3(16)
C(9)−C(10)−C(1A)	125.9(18)	N(1)−C(1)−C(10A)	124.8(16)
N(1)−C(4)−C(5)	126.2(16)	N(2)−C(6)−C(5)	123.6(16)
N(2)−C(9)−C(10)	126.1(16)	N(1)−C(1)−C(2)	110.5(15)
N(1)−C(4)−C(3)	109.3(16)	N(2)−C(6)−C(7)	110.4(15)
N(2)−C(9)−C(8)	107.0(15)	C(2)−C(1)−C(10A)	124.6(18)
C(5)−C(4)−C(3)	124.3(16)	C(5)−C(6)−C(7)	125.9(15)
C(10)−C(9)−C(8)	126.8(18)	C(1)−C(2)−C(3)	107.6(17)
C(2)−C(3)−C(4)	106.2(16)	C(6)−C(7)−C(8)	106.2(15)
C(7)−C(8)−C(9)	109.4(17)	C(4)−C(5)−C(11)	118.7(16)
C(6)−C(5)−C(11)	114.9(16)	C(9)−C(10)−C(17)	116.4(16)
C(14)−N(3)−C(23)	110.7(11)	C(14)−N(3)−C(25)	109.7(12)
C(14)−N(3)−C(27)	110.4(9)	C(19)−N(4)−C(29)	110.4(10)
C(19)−N(4)−C(31)	110.2(10)	C(19)−N(4)−C(33)	111.1(9)

[a] The number in parentheses following each datum is the estimated standard deviation in the last significant figure(s).

This is the second crystal structure of a six-coordinate diaqua water-soluble iron(III) porphyrin, with the only previous crystallographically-characterized diaquairon(III) porphyrins being $[Fe(4\text{-}NMePyP)(H_2O)_2]Cl_5 \cdot 9H_2O$[27] and several forms of the organic solvent-soluble $[FeTPP(H_2O)_2](ClO_4)$.[28−30] All of these structures have an in-plane high-spin ($S = {}^5/_2$) or mixed-spin ($S = {}^5/_2, {}^3/_2$) iron(III) and therefore show lengthening of the Fe−N bonds and concomitant radial expansion of the porphyrin core relative to derivatives with smaller metal ions.[43,44] Thus, the metal−N bonds in all these species have an average distance of >2.02 Å, compared to the distances found for six-coordinate low-spin iron porphyrins (1.990 Å)[44] or for four-coordinate $[Ni(TF_4TMAP)]^{4+}$ (1.928 Å)[38] reflecting the porphyrin core expansion to accommodate the high-spin or admixed-spin iron(III). However, there are differences between the diaquairon porphyrin structures. The structure of $[Fe^{III}(TF_4TMAP)(H_2O)_2](CF_3SO_3)_5 \cdot 2CH_3CN \cdot 2H_2O$ (Fe−N distances 2.042 Å; Fe−O distances 2.09 Å) is most similar to $[Fe(4\text{-}NMePyP)(H_2O)_2]Cl_5 \cdot 9H_2O$ (Fe−N distances 2.042 and 2.038 Å; Fe−O distances 2.086 Å)[27] and the THF-solvated structure [FeTPP-

(43) Scheidt, W. R.; Reed, C. A. *Chem. Rev.* **1981**, *81*, 543−555.
(44) Scheidt, W. R.; Gouterman, M. In *Iron Porphyrins, Part I*; Lever, A. B. P., Gray, H. B., Eds.; Addison-Wesley: Reading, MA, 1983; pp 89−139.

$(H_2O)_2](ClO_4)\cdot 2THF$ (Fe−N distances 2.045 Å; Fe−O distances 2.095 Å),[28] whereas the two nonsolvated $[FeTPP(H_2O)_2](ClO_4)$ structures have significantly smaller porphyrin ring expansions (Fe−N distances 2.024−2.037 Å) and longer Fe−O distances (2.12−2.14 Å).[29,30] These structures indicate that the coordination environment around the high-spin iron(III) is relatively independent of both the electronic structure of the porphyrin and the ortho-phenyl substituents but is dependent on the presence of hydrogen-bonding solvents. The first observation is a little surprising, given that ligands bind to $[Ni^{II}(TF_4TMAP)]^{4+}$ and $[Co^{II}(TF_4TMAP)]^{4+}$ much more readily than to the corresponding TPP derivatives.[38] The second observation indicates that although the F substituents can influence the approach of potential ligands to the metal center they have little direct steric effect on small coordinated ligands. The observation that hydrogen-bonded solvents have such a large effect has been rationalized as being due to hydrogen bonding changing the ligand field at the iron and thereby altering the spin character of the iron center.[29,30] Related effects associated with H-bonding to axial ligands on iron(III) porphyrins have been noted previously.[29,45−47]

The $CF_3SO_3^-$ counterions show a large amount of disorder. The four $CF_3SO_3^-$ anions near the quaternary nitrogens show 2-fold disorder of the F and O atoms, while the fifth $CF_3SO_3^-$ shows equal (50%) occupancy of two sites approximately midway between two iron porphyrins. It is possible that the crystal would be better described in the *P*1 space group, but the data were not deemed of sufficient quality to attempt refinement in the noncentrosymmetric space group.

NMR Behavior as a Function of Water Content in Acetonitrile−Water Mixtures. A previous paper from our group has shown that at 10% (volume/volume, v/v) water in acetonitrile solution the $CF_3SO_3^-$ anion is displaced from the iron(III) center to give the diaqua form of the iron(III) porphyrin as the dominant solution species in acidic solution.[3] There is no evidence for $CF_3SO_3^-$ coordinating to the hydroxo form of the iron(III) porphyrin under any conditions. Solubility considerations lead to the use of the Cl^- salt for H_2O:CH_3CN > 4:1 (v/v) while measurements at lower water content were obtained using the $CF_3SO_3^-$ salt. The different counterions had no discernible effect on the NMR spectra of the monomeric porphyrins at water concentrations where both salts were soluble (50−80% v/v water).

The ^{19}F spectrum of $[Fe(TF_4TMAP)(H_2O)_2]^{5+}$ consists of resonances at ca. −136 and ca. −132 ppm corresponding to the meta fluorines (F″) and the ortho fluorines (F′), respectively. In this species both faces of the porphyrin are identical so that the spectrum is very simple. The ^{19}F resonances for $[Fe(TF_4TMAP)(H_2O)_2]^{5+}$ changed very little over the range of water concentration 10−100%. In contrast, the ortho fluorine ^{19}F NMR resonances for the hydroxo form of the iron(III) porphyrin changed markedly as the water content of the solution was increased from 10% to 100%. Below 70% H_2O $[Fe(TF_4TMAP)OH]^{4+}$ had two ^{19}F NMR signals near −131 and −132 ppm (meta fluorines) and two broad signals near −115 ppm (ortho fluorines), reflecting the inequivalence of the two faces of the porphyrin. At a water concentration of 70−80% the spectrum still shows a broad ortho fluorine signal at ca. −115 ppm but also shows a new broad signal at −120 to −125 ppm. This second signal grows with increasing water content,

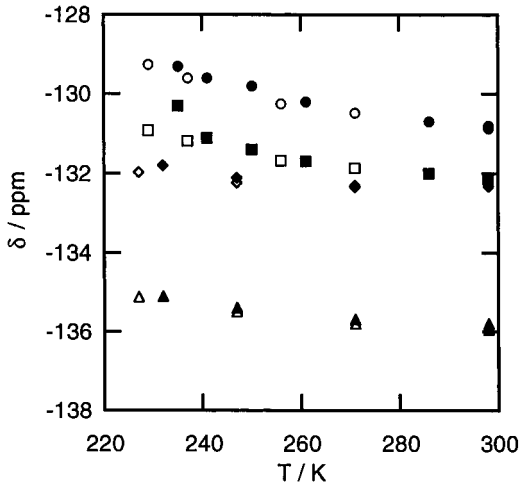

Figure 3. Chemical shifts of ^{19}F NMR resonances observed in the region −128 to −138 ppm as a function of temperature in 5.5 M water in acetonitrile. Open symbols are for experiments in $C^2H_3CN/^1H_2O$ and filled symbols are for experiments in $C^2H_3CN/^2H_2O$: (△, ▲) m-F (F″) of $[Fe^{III}(TF_4TMAP)(H_2O)_2]^{5+}$; (◇, ◆) o-F (F′) of $[Fe^{III}(TF_4TMAP)(H_2O)_2]^{5+}$; (□, ■) m-F (F″) of $[Fe^{III}(TF_4TMAP)OH]^{4+}$; (○, ●) m-F (F″) of $[Fe^{III}(TF_4TMAP)OH]^{4+}$.

while the signal at ca. −115 ppm decreases concomitantly. We assign these peaks to the ortho fluorines of five-coordinate $[Fe(TF_4TMAP)OH]^{4+}$ (ca. −115 ppm) and six-coordinate $[Fe(TF_4TMAP)(H_2O)OH]^{4+}$ (−120 to −125 ppm) on the basis of this change with water concentration. The ^{19}F NMR resonances for the meta fluorines of the hydroxoiron(III) porphyrin showed little dependence on water concentration.

This above analysis of the changes in the ^{19}F NMR resonances for the ortho fluorines of the hydroxoiron(III) porphyrin with changing water concentration is consistent with the observation that as the water content increases the two separate ^{19}F NMR signals for the hydroxoiron(III) porphyrin meta fluorines merge into one peak reflecting equivalence of the two sides of the porphyrin plane on the NMR time scale. This presumably occurs via rapid equilibration of the aqua and hydroxo ligands in $[Fe(TF_4TMAP)(H_2O)OH]^{4+}$. In addition, at higher water concentrations the ^{19}F NMR spectra observed in solutions containing both $[Fe(TF_4TMAP)(H_2O)OH]^{4+}$ and $[Fe(TF_4TMAP)(H_2O)_2]^{5+}$ show average signals rather than the separate peaks observed at lower water concentrations. Averaged signals are also observed for aqueous solutions of other iron(III) complexes of water-soluble porphyrins.[4,33] The ^1H NMR spectrum shows similar behavior as the water concentration increases, with two signals also being observed for the *β*-pyrrole ^1H of the hydroxoiron(III) porphyrin in regions of intermediate water concentration.

The change from five- to six-coordinate geometries was not only dependent on the water concentration. Thus, as additional OH^- was added to a solution with a given water concentration (70−80%) the fraction of the six-coordinate porphyrin $[Fe(TF_4TMAP)(H_2O)OH]^{4+}$ increased compared to $[Fe(TF_4TMAP)OH]^{4+}$. This is different from formation of $[Fe(TF_4TMAP)(OH)_2]^{3+}$, which only occurs at higher concentrations of OH^-.

The variable-temperature studies were all performed at 5.5 M water, where the water content is sufficiently high to displace the weakly-coordinating $CF_3SO_3^-$ ion but is still well below the concentration of water required to cause 6-coordination of the hydroxo porphyrin.

NMR Spectra as a Function of Temperature at Constant Water Content. Figures 3 and 4 show the chemical shifts and line widths observed for the $[Fe(TF_4TMAP)O^1H]^{4+}$, $[Fe(TF_4TMAP)O^2H]^{4+}$, $[Fe(TF_4TMAP)(^1H_2O)_2]^{5+}$, and $[Fe(TF_4TMAP)$-

(45) Momenteau, M.; Mispelter, J.; Lexa, D. *Biochim. Biophys. Acta* **1973**, *320*, 652.
(46) Sweigart, D. A.; Fiske, W. In *Techniques and Applications of Fast Reactions in Solution*; Gettins, W. J., Wyn-Jones, E., Eds.; D. Reidel: Dordrecht, The Netherlands, 1979; pp 315−320.
(47) O'Brien, P.; Sweigart, D. A. *Inorg. Chem.* **1985**, *24*, 1405−1409.

Table 3. Parameters Derived from the Simulations of the ^{19}F VT-NMR Spectra Observed for Solutions of $[Fe^{III}(TF_4TMAP)(H_2O)_2]^{5+}$ and $[Fe^{III}(TF_4TMAP)OH]^{4+}$ in Acetonitrile−Water Solutions

conditions	T (K)	f_{OH}	$10^{-2}\,k'$ (s^{-1})[a]	$10^{-5}\,k''$ ($M^{-1}\,s^{-1}$)[b]	E_a for k'' (kcal mol^{-1})
tot. [porphyrin] = 2.6 mM;	235	0.45	1	0.7	
430 μL of C^2H_3CN/50 μL of ^1H_2O	250	0.42	2.8	2.0	
	261	0.45	5.0	3.5	6.7 ± 0.4
	277	0.45	10.5	7.4	
	284	0.45	13	9	
	298	0.46	22	16	
	312	0.44	44	31	
tot. [porphyrin] = 0.70 mM;	243	0.65	1.5	6.1	
430 μL of C^2H_3CN/50 μL of ^1H_2O	261	0.65	3.0	12	4.8 ± 0.1
	283	0.65	6.0	24	
	298	0.67	9.0	37	
tot. [porphyrin] = 1.5 mM;	246	0.45	0.80	1.0	
400 μL of C^2H_3CN/50 μL of ^2H_2O	261	0.45	2.0	2.5	6.6 ± 0.5
	282	0.45	4.0	5.2	
	298	0.50	9.5	12	

[a] Estimated errors in rate constants: 10%. [b] Values of k'' are calculated from k', assuming that the only process leading to interconversion is a bimolecular process as shown in eq 3.

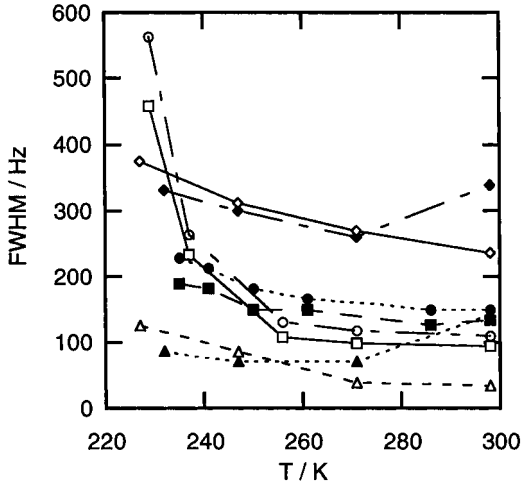

Figure 4. Full widths at half-maximum heights (fwhm) for ^{19}F NMR resonances observed in the region −128 to −138 ppm as a function of temperature in 5.5 M water in acetonitrile. Open symbols are for experiments in $C^2H_3CN/^1H_2O$, and filled symbols are for experiments in $C^2H_3CN/^2H_2O$: (△, ▲) m-F (F″) of $[Fe^{III}(TF_4TMAP)(H_2O)_2]^{5+}$; (◇, ◆) o-F (F′) of $[Fe^{III}(TF_4TMAP)(H_2O)_2]^{5+}$; (□, ■) m-F (F″) of $[Fe^{III}(TF_4TMAP)OH]^{4+}$; (○, ●) m-F (F″) of $[Fe^{III}(TF_4TMAP)OH]^{4+}$.

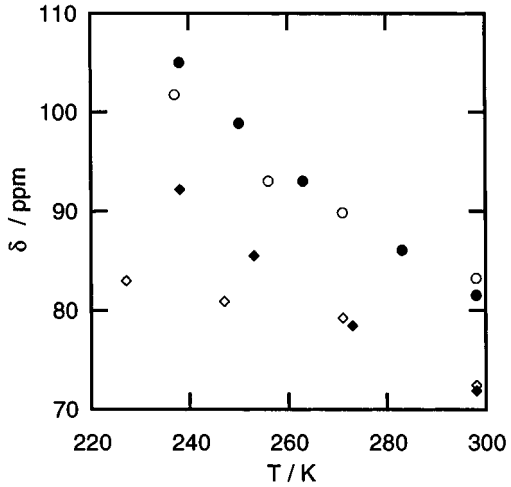

Figure 5. Chemical shifts for the β-pyrrole ^1H NMR resonances of $[Fe^{III}(TF_4TMAP)OH]^{4+}$ in (○) $C^2H_3CN/^1H_2O$ and (●) $C^2H_3CN/^2H_2O$ and of $[Fe^{III}(TF_4TMAP)(H_2O)_2]^{5+}$ in (◇) $C^2H_3CN/^1H_2O$ and (◆) $C^2H_3CN/^2H_2O$ as a function of temperature. All solutions are 5.5 M water in acetonitrile.

$(^2H_2O)_2]^{5+}$ porphyrin ^{19}F resonances in the region −128 to −138 ppm as a function of temperature in 5.5 M H_2O in CH_3CN. The chemical shifts of the ^{19}F resonances all show a Curie T dependence reflecting the paramagnetic nature of the central Fe(III). Measurements of the chemical shift and fwhm values for the separate $[Fe(TF_4TMAP)OH]^{4+}$ and $[Fe(TF_4TMAP)(H_2O)_2]^{5+}$ species agree well with the measurements made on mixtures of the two species at sufficiently low temperatures that equilibration was not occurring. The β-pyrrole ^1H NMR resonance for the $[Fe(TF_4TMAP)OH]^{4+}$ porphyrins moves to higher frequency (lower field) with decrease in temperature, Figure 5, with the deuterated form moving to a greater extent. This may reflect stronger hydrogen-bonding in the deuteriooxo form at low temperatures.

NMR Variable-Temperature Kinetics at Constant Water Content. The variable-temperature (VT) experiment was performed at two concentrations of porphyrin in $C^2H_3CN-^1H_2O$ and at one concentration in $C^2H_3CN-^2H_2O$ (all with 5.5 M H_2O). The details of the simulation analysis are given in the Experimental Section. The ^{19}F NMR resonance frequencies for all the peaks in the absence of exchange were obtained from the above study of the separate aqua and hydroxo porphyrins. This was important because the iron(III) center is paramagnetic and therefore causes significant chemical shift changes and line broadening. Utilization of the experimental values for these parameters accounted for all intramolecular influences of the iron(III) center. The similarity between the observed spectra for the dilute and concentrated porphyrin solutions and the overlap of plots of line width and chemical shift for the separate and mixed solutions at low temperatures, suggest that intermolecular effects were insignificant. The parameters obtained from the fits are given in Table 3, and the fits and experimental data are compared in Figures 6−8. It should be noted from Table 3 that the fraction of $[Fe(TF_4TMAP)OH]^{4+}$ in the samples was almost invariant with temperature (as expected), so that the only controlling variable was the pseudo-first-order rate constant for the reaction, k'. If it is assumed that reaction 5 occurs via the equivalent of reaction 3 (i.e. direct or solvent-mediated proton transfer between porphyrin species, rather than by separate protonation or deprotonation of solvent (cf. reactions 1 and 2)), then it is possible to calculate an apparent second-order rate constant k'' if the porphyrin concentration and f_{OH} are known. These calculated values of k'' are also given in Table 3.

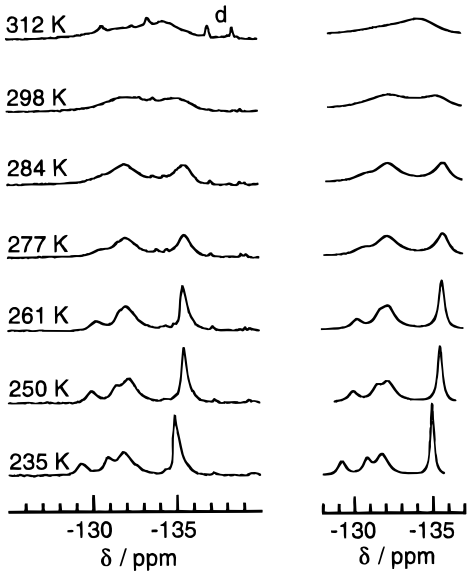

Figure 6. Experimental (left) and simulated (right) ^{19}F NMR spectra in the range −128 to −138 ppm as a function of temperature for 2.6 mM ($[Fe^{III}(TF_4TMAP)(H_2O)_2]^{5+}$ + $[Fe^{III}(TF_4TMAP)OH]^{4+}$) in $C^2H_3CN/^1H_2O$ (d = dimer peaks). All solutions are 5.5 M water in acetonitrile.

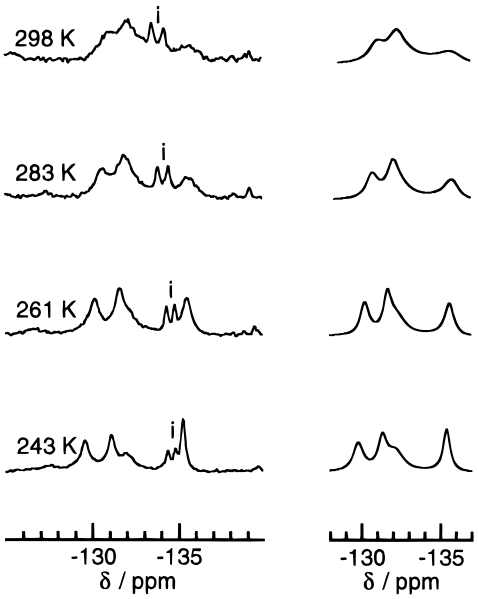

Figure 7. Experimental (left) and simulated (right) ^{19}F NMR spectra in the range −128 to −138 ppm as a function of temperature for 0.70 mM ($[Fe^{III}(TF_4TMAP)(H_2O)_2]^{5+}$ + $[Fe^{III}(TF_4TMAP)OH]^{4+}$) in $C^2H_3CN/^1H_2O$ (i = impurity peaks). All solutions are 5.5 M water in acetonitrile.

Discussion

The initial parts of this study identified the two reactants as being the six-coordinate diaquairon(III) porphyrin $[Fe^{III}(TF_4TMAP)(H_2O)_2]^{5+}$ and the five-coordinate hydroxoiron(III) porphyrin $[Fe^{III}(TF_4TMAP)OH]^{4+}$ at 5.5 M H_2O in acetonitrile. With increasing water content the six-coordinate hydroxoiron(III) porphyrin $[Fe(TF_4TMAP)(H_2O)OH]^{4+}$ becomes more prevalent and is the major form of the hydroxo complex in aqueous solution. The fact that interconversion between $[Fe(TF_4TMAP)(H_2O)_2]^{5+}$ and $[Fe(TF_4TMAP)OH]^{4+}$ is sufficiently slow that it can be followed by NMR spectroscopy can be rationalized by the reactions shown in Scheme 1, which give $K_{a,obs} = [[Fe(TF_4TMAP)OH]^{4+}][H^+][H_2O]/[[Fe(TF_4TMAP)(H_2O)_2]^{5+}] = K_a'K_{aq}'' = K_a''K_{aq}'$. In solutions containing 5.5 M H_2O the complex $[Fe(TF_4TMAP)(H_2O)_2]^{5+}$ is present in higher concentration than $[Fe(TF_4TMAP)(H_2O)]^{5+}$ ($K_{aq}'[H_2O] \gg 1$), while $[Fe(TF_4TMAP)OH]^{4+}$ is more prevalent than $[Fe(TF_4TMAP)(OH)(H_2O)]^{4+}$ ($K_{aq}''[H_2O] \ll 1$). This scheme requires that under these conditions $[Fe(TF_4TMAP)(H_2O)]^{5+}$ is more acidic than $[Fe(TF_4TMAP)(H_2O)_2]^{5+}$, whereas $[Fe(TF_4TMAP)(H_2O)OH]^{4+}$ is more basic than $[Fe(TF_4TMAP)OH]^{4+}$. If the reaction indeed proceeds via $[Fe(TF_4TMAP)(H_2O)]^{5+}$ or $[Fe(TF_4TMAP)(H_2O)OH]^{4+}$, then interconversion will be controlled by the rate of aquation/deaquation, rather than just by the rate of proton transfer. An alternative mechanism of interconversion involves concerted protonation−aquation (or deprotonation-deaquation), with the rate being controlled by the rate of proton-assisted aquation or base-assisted deaquation. Scheme 1 would also suggest that protonation of $[Fe(TF_4TMAP)OH]^{4+}$ with a sufficiently strong acid would be fast and would give $[Fe(TF_4TMAP)(H_2O)]^{5+}$ as the initial product.

The observation that the fraction of hydroxoiron(III) porphyrin in the form $[Fe(TF_4TMAP)(H_2O)OH]^{4+}$ increases both with increased water and with increased base suggests that solvent H_2O or free or metal-bound OH^- hydrogen-bonds to bound H_2O, increasing its donor strength and thereby increasing the concentration of six-coordinate porphyrin. We have noted this effect of the changing donor strength of water in other porphyrin studies, and it is probably related to the fact that the Gutmann donor number for bulk water (33) is much larger than that for monomeric water (18).[48] This effect also militates against using the observed equilibrium between the five- and six-coordinated hydroxoiron(III) porphyrin in water-rich solution to estimate a

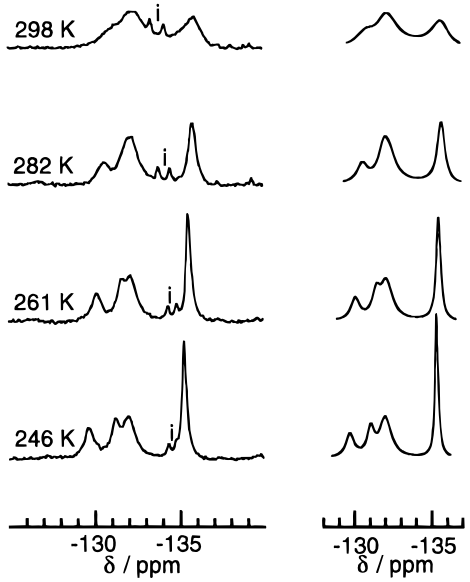

Figure 8. Experimental (left) and simulated (right) ^{19}F NMR spectra in the range −128 to −138 ppm as a function of temperature for 1.5 mM ($[Fe^{III}(TF_4TMAP)(H_2O)_2]^{5+}$ + $[Fe^{III}(TF_4TMAP)OH]^{4+}$) in $C^2H_3CN/^2H_2O$ (i = impurity peaks). All solutions are 5.5 M water in acetonitrile.

Scheme 1. Equilibria between Aquated and Nonaquated Forms of the Iron Porphyrin[a]

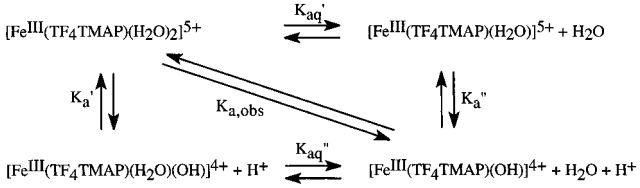

[a] The K_{aq}'s are equilibrium constants for aquation, and the K_a's are acid dissociation constants.

(48) Gutmann, V. *Coord. Chem. Rev.* **1976**, *18*, 225−255.

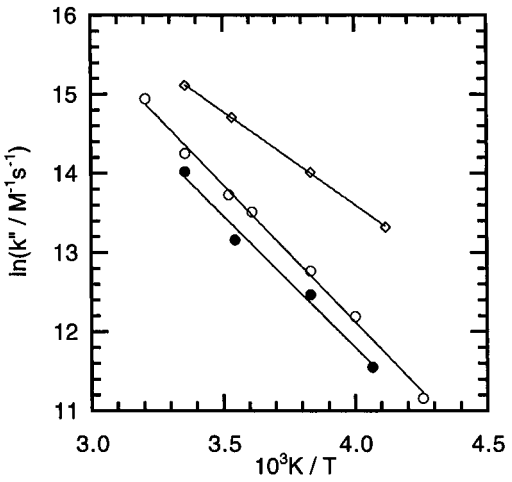

Figure 9. Arrhenius plot of the k'' values reported in Table 3: (○) 2.6 mM ($[Fe^{III}(TF_4TMAP)(H_2O)_2]^{5+}$ + $[Fe^{III}(TF_4TMAP)OH]^{4+}$) in $C^2H_3CN/^1H_2O$; (◇) 0.70 mM ($[Fe^{III}(TF_4TMAP)(H_2O)_2]^{5+}$ + $[Fe^{III}(TF_4TMAP)OH]^{4+}$) in $C^2H_3CN/^1H_2O$; (●) 1.5 mM ($[Fe^{III}(TF_4TMAP)(H_2O)_2]^{5+}$ + $[Fe^{III}(TF_4TMAP)OH]^{4+}$) in $C^2H_3CN/^2H_2O$.

hydration equilibrium constant for use in solutions with a lower water content.

When the water content of the solution increases above 80%, proton transfer becomes rapid, as reflected in the increase of the rate of interconversion of the aqua and hydroxo porphyrins and in the equivalence of the two porphyrin faces in the hydroxo form. The increase in the rate of proton transfer with increasing water content has also been observed for polyoxometalates,[49,50] although in these compounds rate increases have tended to occur at lower water concentrations than noted here.

A plot of the temperature dependence of the calculated apparent second-order rate constants, k'', Figure 9, shows that at the higher concentrations of porphyrin the Arrhenius activation energy is equal within experimental error for the ^1H_2O and ^2H_2O systems. However, the Arrhenius plot of the data for the lower concentration of porphyrin shows curvature and a lower slope, and the derived second-order rate constant is higher than that calculated for the more concentrated solutions. These observations suggest that there is an additional pathway with lower activation energy which becomes more important at low concentrations of porphyrin. Presumably this path involves proton transfer to and from solvent (viz. eq 1 or 2). The equality of the activation energies for the protio and deutero systems suggests that the major determinant of the rate involves distortion of the precursor porphyrin and/or aquation of the iron(III) center, rather than the actual proton transfer. The difference in the rate constants (the k'' values for the protio and deutero systems differ by a factor of 1.4 ± 0.4) suggests that proton transfer is involved in the rate-limiting step. However if the reaction is occurring via protonation and deprotonation of energetically unfavorable intermediates, the activation energy for the proton transfer step is almost certainly much less than the overall activation energy of (6.7 ± 0.5) kcal mol^{-1} while if the protonation (or deprotonation) occurs in a concerted manner the energy of the transition state is very similar for reaction in the presence of ^1H_2O or ^2H_2O.

Three factors are involved in the interconversion between $[Fe^{III}(TF_4TMAP)OH]^{4+}$ and $[Fe^{III}(TF_4TMAP)(H_2O)_2]^{5+}$: exchange of a proton, addition or loss of a coordinated water, and motion of the iron into or out of the porphyrin plane. This last factor is difficult to quantify since there are no crystal structures of iron(III) hydroxo porphyrins, but if it is assumed that the structure of a hydroxo iron(III) porphyrin is similar to a chloro complex, then the iron will be approximately 0.4 Å out of the porphyrin plane[44] while the diaqua iron(III) porphyrin has the iron in the plane. Examination of the experimental results in solutions with higher water content strongly suggests that the interconversion pathway includes $[Fe^{III}(TF_4TMAP)(OH)(H_2O)]^{4+}$ when there is a significant water concentration. However, we cannot exclude the possibility that the paths including the five-coordinate $[Fe^{III}(TF_4TMAP)(H_2O)]^{5+}$ in Scheme 1 are significant when the water concentration is sufficiently low. Finally, it is possible that protonation (or deprotonation) occurs simultaneously with addition (or loss) of axial water. This possibility is represented by the diagonal arrows in Scheme 1.

In conclusion this study has measured the rate of interconversion of $[Fe^{III}(TF_4TMAP)(OH)]^{4+}$ and $[Fe^{III}(TF_4TMAP)(H_2O)_2]^{5+}$ and presents evidence that the reason for the slow interconversion is the change in coordination geometry that accompanies the proton transfer.

Acknowledgment. The authors acknowledge the assistance of Dr. Allan Kershaw with the NMR spectra. We also thank Professor A. Burg for his generous support of our research. This work was partially supported by American Chemical Society Petroleum Research Fund Grant 24256-G3 and by a ZRIF grant from the University of Southern California. T.L. thanks the Department of Education for a graduate fellowship.

Supporting Information Available: Tables of atomic coordinates, anisotropic displacement coefficients, and hydrogen coordinates and a figure showing the rms displacements of the atoms in the porphyrin plane of $[Fe^{III}(TF_4TMAP)(H_2O)_2](CF_3SO_3)_5 \cdot 2CH_3CN \cdot 2H_2O$ (6 pages). Ordering information is given on any current masthead page.

IC961486G

(49) Finke, R. G.; Rapko, B.; Saxton, R. J.; Domaille, P. J. *J. Am. Chem. Soc.* **1986**, *108*, 2947−2960.
(50) Gafarov, S. A.; Chuvaev, V. F. *Azerb. Khim. Zh.* **1988**, 121−125; *Chem. Abstr*. *111*, 141715j.